Strasbourg (France)

MANUSCRIPT COVER PAGE FORM

E-MRS Symposium : Symposium D: Materials Science and Device Issues for Future Si-based Technologies

Paper Number : 2073

Title of Paper : Physically-Based Modeling of Dislocation Loops in Ion Implantation Processing in Silicon

Corresponding Author : Pedro Castrillo

Full Mailing Address : Department of Electronics, University of Valladolid.
ETSIT, Campus Miguel Delibes, E-47011 Valladolid (Spain)

Telephone : 34-983423683 (ext. 5511)

Fax : 34-983423675

E-mail : Pedro.Castrillo@tel.uva.es

Physically-based modeling of dislocation loops in ion implantation processing in silicon

P. Castrillo,[1*] I. Martin-Bragado,[1,2] R. Pinacho,[1] M. Jaraiz,[1] J. E. Rubio,[1]
K. R. C. Mok,[1,3] F. J. Miguel-Herrero,[1] and J. Barbolla[1†]

[1]Department of Electronics, University of Valladolid, ETSIT Campus Miguel Delibes, 47011 Valladolid, Spain

[2]Synopsys. Karl-Hammerschmidt Strasse 34, D-85609 Aschheim/Dornach, Germany

[3]Department of Chemical & Biomolecular Engineering, National University of Singapore. 4 Engineering Drive 4, Singapore 117576

Under certain conditions, particularly for high-dose implants, {311} rod-like defects can evolve into dislocation loops (DLs). In this work, we have developed a model for the transformation of {311} defects into DLs, with a transformation rate that is controlled by a size-dependent energy barrier. The model has been included and calibrated in an atomistic kinetic Monte Carlo simulator. This simulator includes a description of the size distribution of {311}-defects (required for a size-based model) and of the amorphization and recrystallization (needed to provide reliable information on the number of interstitials in the end-of-range region). Extended defects are implemented according to realistic geometries, giving a direct assessment of the correct capture volume for diffusing defects. The model correctly predicts the formation of DLs during the annealing that follows ion implants, both for amorphizing and non-amorphizing conditions, and provides a realistic description of damage morphology. The possible role of stress on DL formation is also discussed.

* E-mail address: Pedro.Castrillo@tel.uva.es
† Recently deceased.

Introduction

Ion implantation is the main doping-technique in silicon-based integrated circuit manufacturing. However, the implanted ions produce a damage in the semiconductor lattice that has to be removed with a subsequent annealing. During the annealing, extended defects nucleate, ripen and eventually dissolve. These extended defects play a crucial role on the dopant diffusion during device processing. In particular, {311}-oriented rod-like defects are known to be the typical source of the interstitial supersaturation during transient enhanced diffusion (TED) [1]. The structure [2] and dissolution behavior [1, 3] of these {311}-defects are well known. Under certain conditions, particularly for high-dose implants, {311}-defects can evolve into dislocation loops (DLs) [4, 5]. This transformation has been observed for both amorphizing [4] and non-amorphizing implants [6]. As DLs are more stable than {311}-defects, their transformation entails a strong decrease of the interstitial supersaturation, drastically slowing down TED [7]. Therefore, for an accurate simulation of the dopant profiles after incomplete anneals, it is crucial to be able to predict whether or not DLs will appear (and when). Moreover, the presence of extended defects in devices would be detrimental for both the reliability and the electrical characteristics and, consequently, it is necessary to estimate the minimum thermal budget to get their complete dissolution. This minimum budget depends on whether stable DLs are formed or not. For all these reasons, the accurate modeling of the transformation of {311}-defects into DLs can play a key role in current silicon process simulation.

At present time, there are good models in the literature for describing the behavior of {311}-defects in low-dose implants, in which no DLs are produced [8, 9, 10]. There are also some models to simulate the growth and ripening of DLs [11] without considering {311}-defects. Concerning the key point of the transformation of {311}-defects into

DLs, it has been treated in two different ways: one assuming a transformation rate that does not depend on defect size [12] and another considering a fixed threshold size for a {311}-defect to unfault into DL [9]. The first one has proved to properly describe the nucleation and evolution of DL in amorphizing implants [12] but, as no size-dependence is considered, it would incorrectly predict DL formation also for low-dose implants, in contradiction with experiments [1, 3]. In contrast, the second one can be used for both low and high doses, elucidating whether or not DLs nucleate and correctly describing the overall evolution of the {311} and DL populations [9]. However, as far as the defect morphology is concerned, transmission electron microscopy (TEM) images show some {311}-defects much larger that the critical size used in the model which have not unfaulted yet [3, 4, 13, 14] and suggest that the transformation is not instantaneous, in contrast with the assumptions of that model.

In this work, we present a model that uses simultaneously the concepts of size dependence and transformation rate and can, thus, account for the stochastic nature of the {311} to DL transition.

Model

Our model bears on the common experimental observation that {311}-defects can reach sizes for which the DL configuration is energetically more favorable. Indeed, the crossover size between the formation energies of {311}-defects and DLs can be estimated to be about 300 interstitials [14] (i.e. less than 20nm in length [1, 8]), whereas much larger {311}-defect sizes, with lengths above 100 nm and containing several thousands of interstitials, can be observed by TEM [3, 4, 13, 14]. This suggests the presence of an energy barrier for the transformation of these metastable {311}-defects into DLs. This energy barrier would be larger for small {311}-defect sizes since no

transformation into DLs is observed for populations of small {311}-defects [1]. The idea of a thermally activated transformation is also supported by the fact that, for similar sizes, the transformation is more difficult (less frequent) at lower temperatures [2, 14]. From a microscopic point of view, the energy barrier for the transformation reflects the difficulty of rearranging a large extended defect.

The energy barrier as a function of size that we have used is represented in Fig.1a. This gives a size-dependent transformation rate at 800ºC as shown in Fig.1b, where a rate prefactor of $4.5 \cdot 10^{11}$ s^{-1} has been used. In order to illustrate the global effect of size dependence, let us assume, for example, two different populations of {311}-defects with size distributions like those of Fig.1c, both following log-normal distributions [16], one with smaller defects (with a mean size of 300 interstitials and a mean length of about 18 nm) and the other with larger defects (with 2500 interstitials and ~75 nm length on average). The products of the rate and the size distributions are in Fig.1d. The areas under the curves correspond to the total transformation rates, which would be much faster for the case of the larger size population. (The average transformation times would be about 10 minutes and 7 hours, respectively).

Implementation

We have included the model described above in the atomistic kinetic Monte Carlo (kMC) simulator DADOS [17, 18]. We take advantage of the ability of the kMC method to incorporate multiple mechanisms and interactions in a detailed yet simple way. The simulator provides an excellent description of the amorphization and recrystallization [19], which will be needed to provide reliable information on the number of interstitials in the end-of-range region in amorphizing conditions.

Extended defects have been implemented according to realistic geometries, giving a direct assessment of the capture volume for diffusing defects. {311}-defects have been arranged in any of the twelve equivalent orientations, with the areal density derived from high resolution microscopy (5 interstitials/nm^2) [2] and with lateral width increasing with length [8, 20, 21]. In particular, we have used the relationship $W = \sqrt{0.5nm \cdot L}$ [8, 20]. DLs have been implemented assuming that they are of the faulted type, which is known to be the dominant variety of DLs for diameters smaller than 80 nm [15]. Consequently, DLs have been arranged with disk shape in any of the {111} orientations, with areal density of 15.7 interstitials/nm^2 [15]. The energetics of DLs has been taken from elastic and dislocation theory [15] and their emission prefactor has been adjusted to fit the experimental interstitial supersaturation [7].

Concerning {311}-defects and small clusters the simulator provides a good fit of their dissolution [1, 8] and of the supersaturation they cause [22] (see Ref.[18]). A good description of size evolution is also achieved [1, 8], which is essential for a size-based model. There are many other features that arise in a natural way from the simulations, such as the depth distribution or the two regimes dissolution behavior experimentally reported in Ref.[3]. We would like to remark that, in agreement with experiments, no transformation of {311}-defects into DLs is observed when simulating the low dose implants of Refs.[1, 3].

Simulation results

We now discuss some examples of simulations corresponding to experiments reported in the literature. The first one corresponds to a room temperature 100 KeV Si^+-implant, with a dose of $2 \cdot 10^{14}$ cm^{-2} and a dose rate of $2.5 \cdot 10^{13}$ cm^{-2} s^{-1}, followed by 800ºC anneal [4, 13]. These implant conditions are a non-amorphizing, as confirmed by cross-section

TEM [13]. The simulation of the implant process, including dynamic annealing, confirms the lack of a continuum amorphous layer but reveals the presence of small disordered regions with a depth distribution in correspondence with the dark spots observed by TEM. During the subsequent annealing, {311}-defects are formed and they are observed in-situ to evolve into DLs [4]. The experimental time evolution of the interstitials in both types of defects is displayed in Fig.2. The simulation results (also shown in the figure) correctly reproduce the transformation timing of {311}-defects into DLs. However the number of interstitials in defects seen by microscopy is only a 35% of the amount obtained in the simulation, and the simulated curves in the figure have been scaled by this factor. We have explored several hypotheses to explain such discrepancy (unstable small interstitial clusters acting as bottleneck, interstitial capture by carbon traps, microscopy resolution limitations, etc) but no conclusive explanation has been found so far. We would like to point out that no simplifying assumptions about the initial damage (like the "+1 model" [23]) have been made in our simulations and the number of interstitials in extended defects that we get is close to one interstitial per implanted ion (supporting the validity of the "+1 model" for the present conditions).

Figures 3a and 3b show the TEM plan-views corresponding to the experiment of Fig.2. after 10 and 20 minutes at 800ºC, taken from Ref.[13]. Figures 3c and 3d show our simulated configurations for the same conditions. Both micrographs and simulations are in the same scale (200 nm × 200 nm) and orientation (with borders aligned along <001> directions). A good resemblance is found between the morphology observed by TEM and the calculated in our simulations. (These "simulated pictures" do not include calculations of the diffraction intensity but only the simulated coordinates of the particles. Therefore, no quantitative comparison with the TEM contrast can be done). It is interesting to notice that in Fig.3c small DLs (that have transformed at relatively

small sizes) coexist with large {311}-defects that have not transformed into DLs yet. This illustrates the fact that in our model there is not just a “threshold size” for the transformation from {311}-defects to DLs but a size-dependent transformation rate. A remarkable observation is that {311}-defects that appear elongated along the [010] and [001] directions in the (100) projection (i.e., horizontally and vertically in Fig.3c) are not seen in the TEM micrograph of Fig.3a and yet hold nearly two thirds of the total number of interstitials in Fig.3c (although their high tilt angle makes them look thinner and shorter). This could be one of the possible reasons for the scaling factor needed in Fig.2. The comparison between Figs.3c and 3d, corresponding to the same simulated region at different anneal times, illustrates the evolution of individual extended defects: some {311}-defects dissolve whereas others grow and/or transform into DLs, while DLs formed at early times experience a noticeable ripening.

Simulations performed for the same implant energy and annealing temperature of the experiment of Figs. 2 and 3, but lowering the dose, indicate that the onset dose for DL formation is about 10^{14} cm^{-2}, in agreement with recent experiments [24].

Figure 4 represent the time evolution of DLs and {311}-defects during the annealing that follows an amorphizing Si^+ implant [6]. The implant energy is 20 keV, the dose and dose rate are 10^{15} cm^{-2} and $1.9 \cdot 10^{15}$ cm^{-2} s^{-1} respectively, and the annealing has been performed at 750ºC. Although the conditions are rather different from the previous case, a good qualitative agreement is observed again between the experimental data and the simulations. A correction factor of 0.5 (close to the 0.35 of Fig.2) is needed in this case to account for the lower amount of interstitials observed in the experiment compared to the simulation.

Some unexplained cases

Although the model that we have presented for the formation of DLs seems to be applicable in a wide range of conditions, there are some extreme situations in which the underlying phenomenology may be substantially different. In particular, no {311}-defect formation but direct DL nucleation can occur for very shallow (5 KeV) Ge^+ implants [25] as well as for very high dose amorphizing implants [26]. This different behavior could be related to the effect of stress, induced by high-defect density and affected by surface proximity. In fact, stress is expected to modify the energetics of extended defects, affecting both the crossover-size of formation energies of {311}-defects and DLs and the energy barrier for the transformation between both. Additionally, the emission rates and, therefore, the ripening and dissolution rates might be also affected. Therefore, the inclusion of stress in our modeling framework would be desirable in order to expand the range of conditions in which the simulations can be really predictive. A coherent stress assessment should include the reciprocal influence between the stress field and the extended defects: the stress would modify the energetics of extended defects and conversely the extended defects would produce a local stress field.

In addition to stress, chemical effects related to the Ge fraction in relaxed SiGe alloys has been reported to modify both the extended-defect dissolution and the DL nucleation path [27].

Conclusions

In summary, we have presented a physically-based model for the transformation of {311}-defects into DLs considering a size-dependent energy barrier. The model has been implemented in an atomistic kMC simulator that includes a comprehensive treatment of ion-induced damage evolution and realistic geometries and energetics for

extended defects. The model has been tested both for amorphizing and non-amorphizing conditions, and provides a realistic 3D description of damage morphology. Reciprocal influence between stress and extended defects is desirable to be included in the near future.

This work has been partially supported by the Spanish Government under project BFM2001-2250 and by the Castilla y Leon regional Government under project VA-070A05

References

1. D.J. Eaglesham, P.A. Stolk, H.J. Gossman, and J.M. Poate, Appl. Phys. Lett., 65 (1994) 2305.

2. S. Takeda, Jpn. J. Appl. Phys., 30 (1991) 639.

3. N. Cherkashin, P. Calvo, F. Cristiano, B. de Mauduit, and A. Claverie, Mat. Res. Soc. Symp. Proc., 810 (2004) 103.

4. J.-H. Li and K.S. Jones, Appl. Phys. Lett., 73 (1998) 3748.

5. A. Claverie, B. Colombeau, G.B. Assayag, C. Bonafos, F. Cristiano, M. Omri, and B. de Mauduit, Mater. Sci. Semicond. Process., 3 (2000) 269.

6. S. Robertson, K.S. Jones, L.M. Rubin, and J. Jackson, J. Appl. Phys., 87 (2000) 2910.

7. C. Bonafos, M. Omri, B. de Maudit, G. B. Assayag, A. Claverie, D. Alquier, A. Martinez, and D. Mathiot, J. Appl. Phys., 82 (1997) 2855.

8. G. Hobler and C.S. Rafferty, Mat. Res. Soc. Symp. Proc., 568 (1999) 123.

9. H. Gencer and S.T. Dunham, J. Appl. Phys., 91 (2002) 2883.

10. A. Claverie, B. Colombeau, F. Cristiano, A. Altibelli, and C. Bonafos, Nucl. Instr. and Meth. B, 186 (2002) 281.

11. E. Lampin, V. Senez, and A. Claverie, J. Appl. Phys., 85 (1999) 8137.

12. I. Avci, M.E. Law, E. Kuryliw, A.F. Saavedra, and K.S. Jones, J. Appl. Phys., 95 (2004) 2452.

13. J.-H. Li, M.E. Law, C. Jasper, and K.S. Jones, Mater. Sci. Semicond. Process., 1 (1998) 99.

14. P. Calvo, A. Claverie, N. Cherkashin, B. Colombeau, Y. Lamrani, B. de Maudit, and F. Cristiano, Nucl. Instr. and Meth. B, 216 (2004) 173.

15. F. Cristiano, J. Grisolia, B. Colombeau, M. Omri, B. de Maudit, A. Claverie, L. F. Gilles, and N. E. B. Cowern, J. Appl. Phys., 87 (2000) 8420.

16. G.Z. Pan and K.N. Tu, J. Appl. Phys., 82 (1997) 601.

17. M. Jaraiz, L. Pelaz, E. Rubio, J. Barbolla, D.J. Eaglesham, H.-J. Gossmann, and J.M. Poate, Mat. Res. Soc. Symp. Proc. 532 (1998) 43.

18. M. Jaraiz, in J. Dabrowski and E.R. Weber (Eds), Predictive Simulation of Semiconductor Processing, Springer-Verlag, Berlin, 2004, p.73.

19. M.C. Mok, M. Jaraiz, I. Martin-Bragado, J E. Rubio, P. Castrillo, R. Pinacho, M.P. Srinivasan, and F. Benistant, Mater. Sci. Eng. B, in the press.

20. J. Liu, PhD thesis, University of Florida, Gainesville, FL (1997).

21. G. Subramanian, K.S. Jones, M.E. Law, M.J. Caturla, S. Theiss, and T.D. de la Rubia, Mat. Res. Soc. Symp. Proc., 610 (2001) B11.10.

22. N.E.B. Cowern, G. Mannino, P.A. Stolk, F. Roozeboom, H.G.A. Huizing, J.G.M. van Berkum, F. Cristiano, A. Claverie, and M. Jaraiz, Phys. Rev. Lett. 82, 4460 (1999).

23. M.D. Giles, J. Electrochem. Soc. 138 (1991) 285.

24. IST Project 2000-30129, Front-End Models for Silicon Future Technology (FRENDTECH), Public Final Report (2004).

25. F. Gutierrez, K.S. Jones, and D.F. Downey, Mat. Res. Soc. Symp. Proc., 669 (2001) J5.11.

26. J. Liu, M.E. Law, and K.S. Jones, Solid State Electron., 38 (1995) 1305.

27. R. Crosby, K.S. Jones, M.E. Law, A. Nylandsted Larsen, and J. Lundsgaard Hansen, Mater. Sci. Semicond. Process., 6 (2003) 205.

Figure captions.

Figure 1. (a) Energy barrier for the transformation from {311}-defects to DLs as a function of size (number of interstitials, N) used in our simulations. The resulting transition rate, R(N), at 800ºC is plotted in (b). As an example, the size distributions, g(N), of two different defect populations are displayed in (c) and their transformation rates per unit size, R(N)×g(N), are displayed in (d).

Figure 2. Time evolution of the interstitial concentration in extended defects for the 800ºC anneal that follows a non-amorphizing 100 keV, $2 \cdot 10^{14}$ Si^{+}-implant. Experimental data (squares: {311}-defects, circles: DLs) are from Ref.[4]. Simulation results are plotted as lines (dashed: {311}-defects, solid: DLs). Simulated results have been scaled by a factor of 0.35. See discussion in the text.

Figure 3. Plan-view of {311}-defects and DLs corresponding to the anneal of Fig.2. (a)-(b): TEM images, reproduced (with permission) from Ref.[13] [Li *et al.*, Mater. Sci. Semicond. Process. 1 (1998) 99]. (c)-(d): kMC simulations. (a) and (c) are for 10 minutes anneal whereas (b) and (d) are for 20 minutes anneal.

Figure 4. Interstitial concentration in extended defects as a function of time for the 750ºC annealing after an amorphizing 20 keV, 10^{15} Si^{+}-implant. Experimental data (squares: {311}-defects, circles: DLs) are from Ref.[6]. Simulation results are plotted as lines (dashed: {311}-defects, solid: DLs). Simulated results have been scaled by a factor of 0.5.

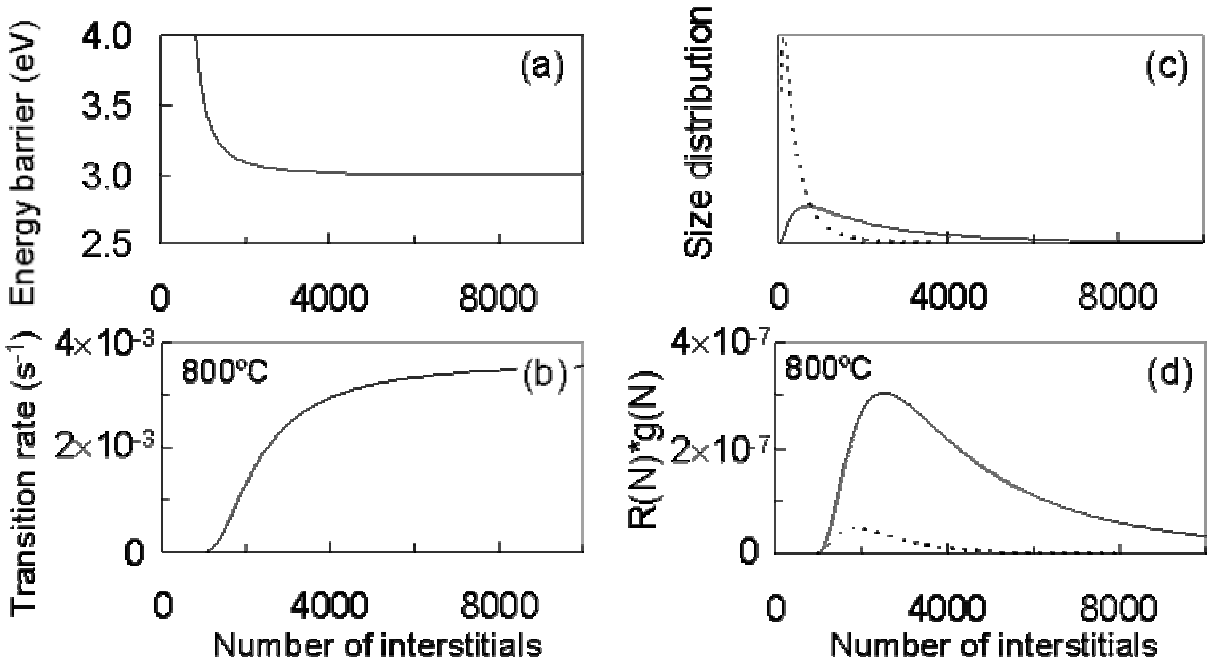
Energy barrier (eV)
4.0
3.5
3.0
2.5
(a)
0
4000
8000
Transition rate (s^{-1})
4×10^{-3}
2×10^{-3}
0
800ºC
(b)
0
4000
8000
Number of interstitials
Size distribution
(c)
0
4000
8000
R(N)*g(N)
4×10^{-7}
2×10^{-7}
0
800ºC
(d)
0
4000
8000
Number of interstitials

Figure 1

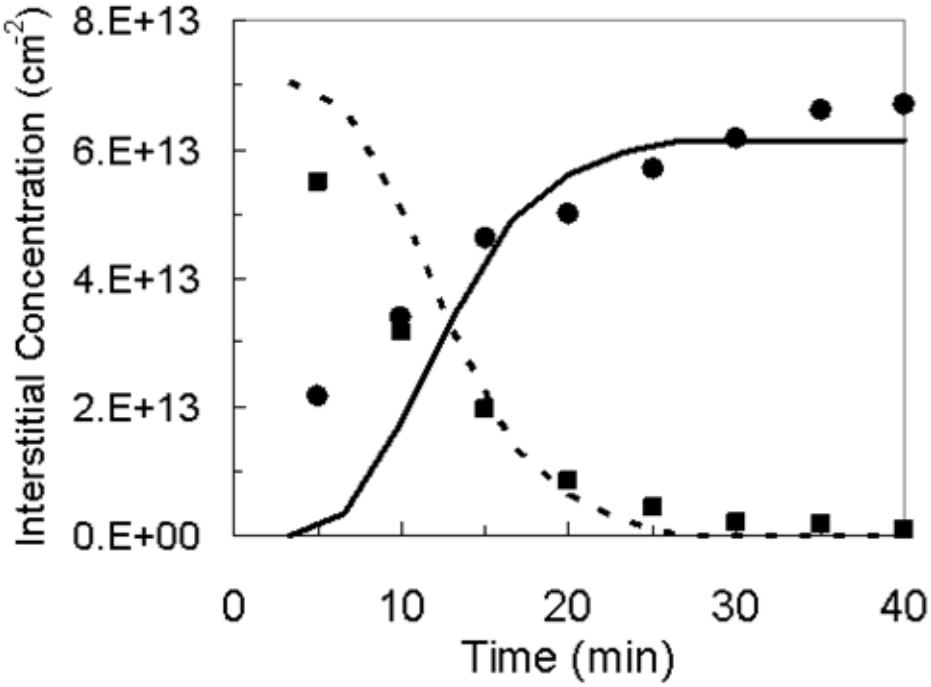
Interstitial Concentration (cm-2)
8.E+13
6.E+13
4.E+13
2.E+13
0.E+00
0
10
20
30
40
Time (min)

Figure 2

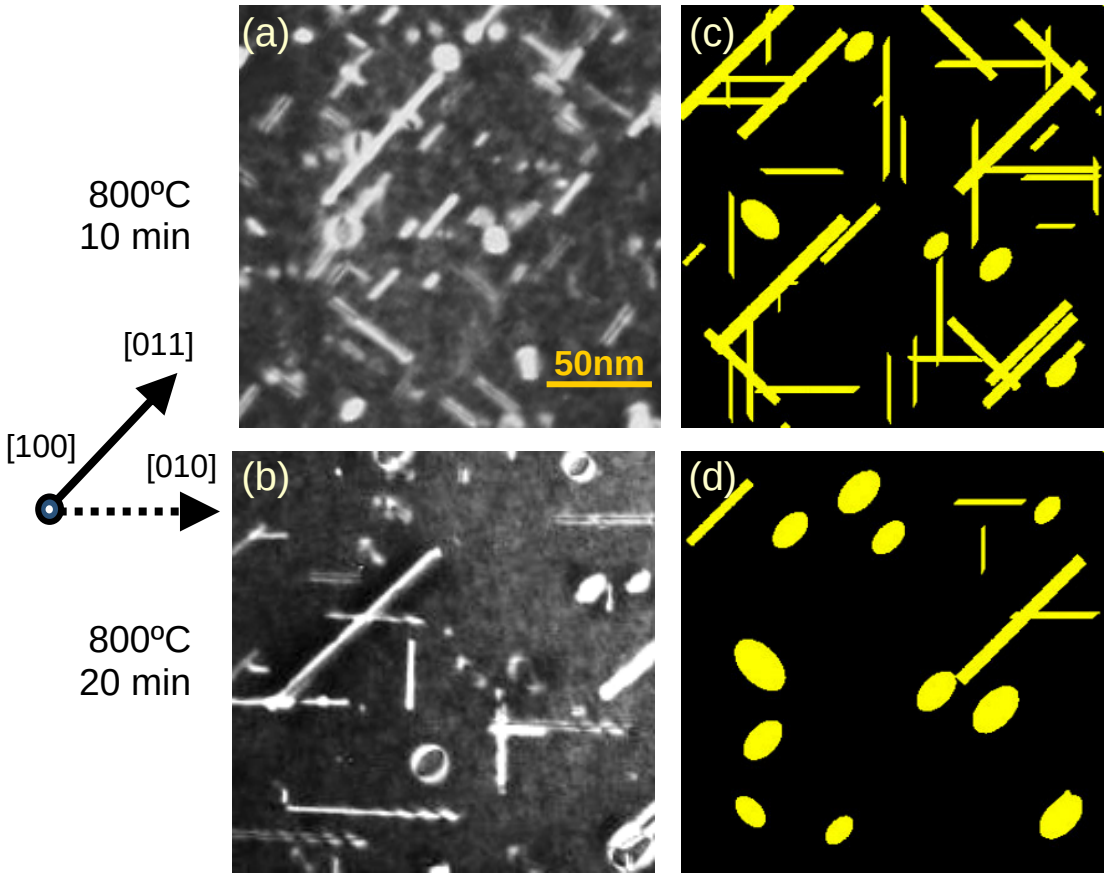

Figure 3

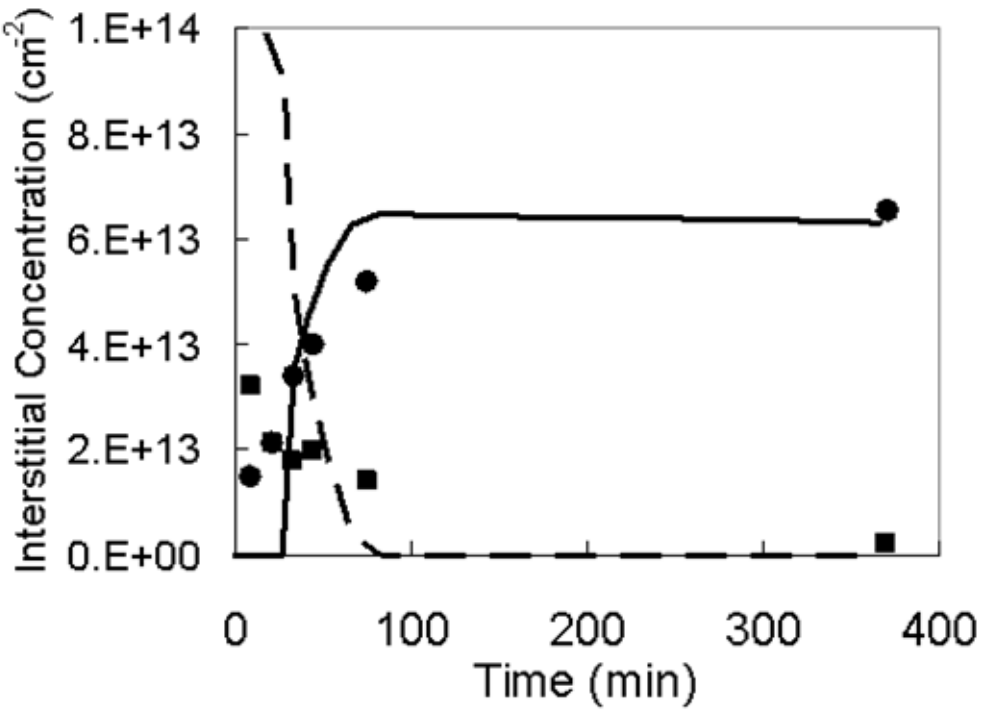
Interstitial Concentration (cm-2)
1.E+14
8.E+13
6.E+13
4.E+13
2.E+13
0.E+00
0
100
200
300
400
Time (min)

Figure 4